Chinese Chemical Letters 36 (2025) 110611

Contents lists available at ScienceDirect

Chinese Chemical Letters

journal homepage: www.elsevier.com/locate/cclet

Graphene-supported isolated platinum atoms and platinum dimers for CO_2 hydrogenation: Catalytic activity and selectivity variations

Sanmei Wang [a,b,c,1], Dengxin Yan [d,1], Wenhua Zhang [c,d,*], Liangbing Wang [b,*]

[a] Research Institute of Interdisciplinary Sciences (RISE) and School of Materials Science & Engineering, Dongguan University of Technology, Dongguan 523808, China
[b] State Key Laboratory for Powder Metallurgy, School of Materials Science and Engineering, Central South University, Changsha 410083, China
[c] Hefei National Laboratory for Physical Sciences at the Microscale and Synergetic Innovation Centre of Quantum Information & Quantum Physics, University of Science and Technology of China, Hefei 230026, China
[d] Laboratory for Chemical Technology, Ghent University, Ghent 9052, Belgium

ARTICLE INFO

Article history:
Received 11 September 2024
Revised 31 October 2024
Accepted 4 November 2024
Available online 5 November 2024

Keywords:
CO_2 hydrogenation
Graphene
Pt single-atom
Pt_2 dimers
DFT

ABSTRACT

Manipulating catalyst structures to control product selectivity while maintaining high activity presents a considerable challenge in CO_2 hydrogenation. Combining density functional theory calculations and microkinetic analysis, we proposed that graphene-supported isolated Pt atoms (Pt_1/graphene) and Pt_2 dimers (Pt_2/graphene) exhibited distinct selectivity in CO_2 hydrogenation. Pt_1/graphene facilitated the conversion of CO_2 into formic acid, whereas Pt_2/graphene favored methanol generation. The variation in product selectivity arose from the synergistic interaction of Pt_2 dimers, which facilitated the migration of H atoms between two Pt atoms and promoted the transformation from *COOH intermediates to *$C(OH)_2$ intermediates, altering the reaction pathways compared to isolated Pt atoms. Additionally, an analysis of the catalytic activities of three Pt_1/graphene and three Pt_2/graphene structures revealed that the turnover frequencies for formic acid generation on Pt_{1ii}/graphene and methanol generation on Pt_{2i}/graphene were as high as 744.48 h^{-1} and 789.48 h^{-1}, respectively. These values rivaled or even surpassed those previously reported in the literature under identical conditions. This study provides valuable insights into optimizing catalyst structures to achieve desired products in CO_2 hydrogenation

The depletion of fossil fuels and climate change are two major problems we face today, so reducing greenhouse gas emissions and finding alternative carbon sources is urgent [1–3]. Converting CO_2 into value-added chemicals [4–7] like methanol (CH_3OH) and formic acid (HCOOH) presents an intriguing approach to both generating renewable energy and mitigating greenhouse gas concentrations [8–11]. Nevertheless, the process of CO_2 hydrogenation poses a significant challenge due to the thermodynamic and kinetic stability of CO_2 [12,13]. To enhance the conversion rate of CO_2 and the selective production of desired products, the development of high-performance catalysts is essential.

Atomically dispersed catalysts, such as single-atom catalysts (SACs) [14–19] and dual-atom catalysts (DACs) [19–24], have been widely employed in CO_2 reduction reaction (CO_2RR) and have shown variations in catalytic activity and selectivity. For example, Shi *et al.* [19] reported that Cu/PCN SACs favored the desorption of *CO to generate CO products, while InCu/PCN DACs promoted the coupling of two *CO intermediates to form ethanol through the synergistic effect of In-Cu. Ren *et al.* [25] discovered that Ni/Fe-NC DACs demonstrated superior CO_2RR performance for CO production compared to Fe SACs and Ni SACs. The CO selectivity remained above 90% across a wide potential range from −0.5 V to −0.9 V. Wang *et al.* [26] observed that Fe_2-N-C electrocatalyst achieved an enhanced CO Faradaic efficiency exceeding 80% across broader potential ranges, with a higher turnover frequency and improved durability compared to SAC counterparts. Sun *et al.* [27] reported that the Faradaic efficiency for CO_2-to-C_2H_4 over Cu_2/NC reached up to ~34.9% at a current density of 33.6 mA/cm^2, whereas its Cu single-atom counterpart exclusively produced CO without yielding C_2H_4. Despite extensive and ongoing efforts to investigate the application of DACs and SACs in CO_2 conversion, further research is still required to fully understand the catalytic differences between SACs and DACs in CO_2 hydrogenation and to advance the development of efficient catalysts.

* Corresponding authors.
E-mail addresses: whhzhang@ustc.edu.cn (W. Zhang), wanglb@csu.edu.cn (L. Wang).
[1] These authors contributed equally to this work.

https://doi.org/10.1016/j.cclet.2024.110611
1001-8417/

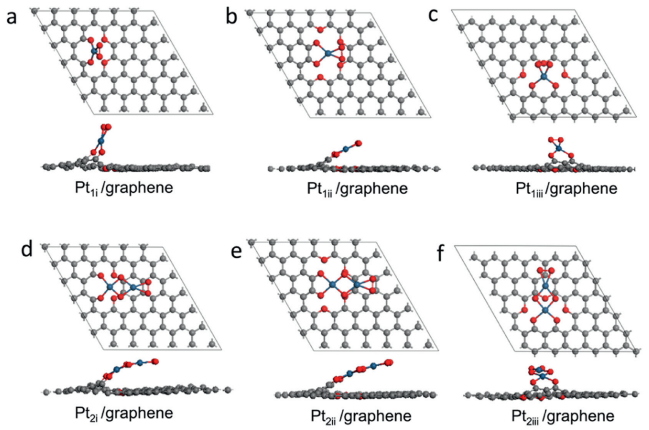

Fig. 1. The structures of (a) Pt_{1i}/graphene, (b) Pt_{1ii}/graphene, (c) Pt_{1iii}/graphene, (d) Pt_{2i}/graphene, (e) Pt_{2ii}/graphene, and (f) Pt_{2iii}/graphene adsorbing $^*O_2$ molecules. The navy blue, grey, and red spheres represented Pt, C, and O atoms, respectively.

Pt-based catalysts have been widely used in various reactions due to their superior activity [28–30], and Pt SACs and Pt DACs exhibit different catalytic activities. For example, a recent study reported that Pt_2 dimers formed on graphene (Pt_2/graphene) displayed a ~17-fold higher catalytic activity than graphene supported Pt single atoms (Pt_1/graphene) in hydrolytic dehydrogenation of ammonia borane [31]. Inspired by this, we ponder whether Pt_2/graphene outperforms Pt_1/graphene in CO_2 hydrogenation. Clarifying this is beneficial for expanding the potential applications of atomically dispersed catalysts in chemical reactions. Herein, in this work, we investigated the catalytic performance of Pt_1/graphene and Pt_2/graphene for CO_2 hydrogenation by using density functional theory (DFT) calculations and microkinetic analysis. Results indicated that Pt_1/graphene and Pt_2/graphene exhibited significant differences in the catalytic properties for CO_2 hydrogenation. Pt_1/graphene tended to produce HCOOH, whereas Pt_2/graphene facilitated the conversion of CO_2 into CH_3OH. Additionally, the turnover frequencies (TOF) of the top-performing structures among the three configurations of Pt_1/graphene and Pt_2/graphene were predicted to reach as high as 744.48 h^{-1} and 789.48 h^{-1}, respectively, demonstrating their exceptional catalytic activity in CO_2 hydrogenation.

According to previous studies [31], Pt_1/graphene was synthesized under O_2 environments, leading to the chemisorption of O_2 molecules on Pt atoms and the presence of two O atoms at the interface. In contrast, the synthesis of Pt_2/graphene in O_3 environments resulted in the formation of Pt_2O_6 chain structures, where the O atoms alternate between terminal and bridge positions. The specific structures of Pt_1/graphene and Pt_2/graphene depended on both the size of the C-vacancy and the configuration of the two interfacial O atoms. Based on these findings, we established three distinct models for Pt_1/graphene and Pt_2/graphene, respectively, and investigated their catalytic performance for CO_2 hydrogenation.

As shown in Fig. 1, three Pt_1/graphene models were identified as Pt_{1i}/graphene, Pt_{1ii}/graphene, and Pt_{1iii}/graphene. Pt_{1i}/graphene featured a single Pt atom supported on the armchair edge of graphene, where the Pt atom was situated within a seven-membered ring composed of one Pt atom, two O atoms, and four C atoms (Fig. 1a). Pt_{1ii}/graphene showcased a single Pt atom supported on the armchair edge of graphene, where the Pt atom was located within a five-membered ring consisting of one Pt atom, two O atoms, and two C atoms (Fig. 1b). Pt_{1iii}/graphene exhibited a single Pt atom supported on the zigzag edge of graphene, where the Pt atoms were positioned within a six-membered ring comprising one Pt atom, two O atoms, and two C atoms (Fig. 1c). Pt_2/graphene configurations were constructed based on the corresponding Pt_1/graphene, with the end-adsorbed $^*O_2$ molecule being replaced by 2O-Pt-O_2 to form a lattice structure. These three Pt_2/graphene configurations were labeled as Pt_{2i}/graphene, Pt_{2ii}/graphene, and Pt_{2iii}/graphene, as shown in Figs. 1d-f, respectively.

After establishing the catalyst structures, we initially treated them with H_2 to remove the chemisorbed $^*O_2$ from the structures. The free energy profiles for the reaction of $^*O_2$ with H_2 over Pt_{1i}/graphene, Pt_{1ii}/graphene, Pt_{1iii}/graphene, Pt_{2i}/graphene, Pt_{2ii}/graphene, and Pt_{2iii}/graphene were displayed in Figs. S1, S3-S6, and S8 (Supporting information), respectively. For Pt_1/graphene structures, the Pt atoms act as the active sites, while for Pt_2/graphene configurations, the top Pt atoms (named as Pt_{top}) served as the active sites for the reaction between $^*O_2$ and H_2. After the reaction of $^*O_2$ with H_2, $^*O_2$ in the Pt_1/graphene and Pt_2/graphene structures were removed in the form of H_2O molecules, and the Pt active sites were occupied by two $^*H$ species (Fig. S9 in Supporting information).

The two H species on Pt sites may transfer to adjacent O atoms. To illustrate this phenomenon, we chose Pt_{1ii}/graphene and Pt_{2ii}/graphene as examples for analyzing the energy barriers associated with H transfer. The calculated values for Pt_{1ii}/graphene and Pt_{2ii}/graphene were 1.44 eV (Fig. S10 in Supporting information) and 0.42 eV (Fig. S11 in Supporting information), respectively. The results suggested that the migration of H from Pt sites to O atoms was relatively challenging on Pt_{1ii}/graphene, whereas it was remarkably straightforward on Pt_{2ii}/graphene. After the H on the Pt_{top} sites of Pt_{2ii}/graphene migrated to O atoms, an H_2 molecule dissociated into two H species and then transferred to the O atoms with an energy barrier of 0.85 eV (Fig. S11).

Based on the above analysis, we concluded that after Pt_1/graphene with O_2 adsorption was treated with H_2, it ultimately transformed into a 2H-Pt_1/graphene structure, where the Pt site was occupied by two $^*H$ species, as depicted in Figs. S12a-c (Supporting information). For Pt_2/graphene with O_2 adsorption, after H_2 treatment, it eventually transformed into a 2H-2OH-Pt_2/graphene structure, where the Pt_{top} site was occupied by two $^*H$ species, and the bridge oxygen between the two Pt coordinated with the H species, as shown in Figs. S12d-f (Supporting information). Subsequently, we introduced CO_2 molecules to explore the process of CO_2 conversion.

For 2H-Pt_1/graphene, CO_2 molecules were firstly adsorbed on Pt atoms, and the adsorption free energies of CO_2 on 2H-Pt_{1i}/graphene, 2H-Pt_{1ii}/graphene, and 2H-Pt_{1iii}/graphene were 0.48, 0.71, and 0.56 eV, respectively. The liner ∠O–C-O on 2H-Pt_{1i}/graphene, 2H-Pt_{1ii}/graphene, and 2H-Pt_{1iii}/graphene was shrunk to 142.04°, 145.06°, and 139.62°, respectively. The adsorption of CO_2 was followed by hydrogenation to form $^*COOH$ or $^*HCOO$ intermediates. The energy barriers for the formation of $^*COOH$ over 2H-Pt_{1i}/graphene, 2H-Pt_{1ii}/graphene, and 2H-Pt_{1iii}/graphene were 0.51, 0.50, and 0.39 eV, respectively, which were lower than that for $^*HCOO$ generation with energy barriers of 1.09, 0.86, and 0.92 for 2H-Pt_{1i}/graphene, 2H-Pt_{1ii}/graphene, and 2H-Pt_{1iii}/graphene, respectively. The result indicated that $^*CO_2$ tended to hydrogenate into $^*COOH$ species on 2H-Pt_1/graphene.

The $^*COOH$ species were unstable and may directly combine with $^*H$ to produce $^*HCOOH$. The energy barriers for hydrogenation of $^*COOH$ to $^*HCOOH$ over 2H-Pt_{1i}/graphene, 2H-Pt_{1ii}/graphene, and 2H-Pt_{1iii}/graphene were 1.90 eV (Fig. S13 in Supporting information), 1.92 eV (Fig. 2), and 1.34 eV (Fig. S14 in Supporting information), respectively, indicating that direct hydrogenation of $^*COOH$ with $^*H$ to form $^*HCOOH$ was unlikely. Instead, it was more likely that an H_2 molecule dissociated into two $^*H$ atoms firstly, followed by the combination of $^*COOH$ and

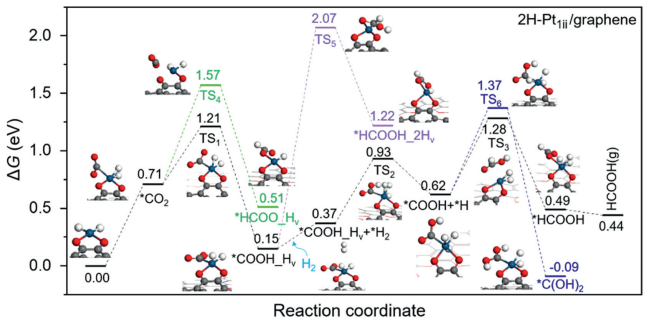

Fig. 2. The free energy profiles for CO_2 hydrogenation to HCOOH on 2H-Pt_{1ii}/graphene. TS represented the transition state. The black route was the most likely reaction pathway. The navy blue, grey, white, and red spheres represented Pt, C, H, and O atoms, respectively. H_v represented one H atom was missing from 2H-Pt_{1ii}/graphene structure after it binds to $^*CO_2$ or $^*COOH$ intermediate.

$^*H$ to form $^*HCOOH$. Thus, we investigated the dissociation of H_2 molecules in the presence of $^*COOH$. For 2H-Pt_{1i}/graphene (Fig. S13), the energy barrier for H_2 dissociation was 1.22 eV, which was lower than that for direct hydrogenation of $^*COOH$ to $^*HCOOH$ (1.90 eV). A similar phenomenon was observed for 2H-Pt_{1ii}/graphene and 2H-Pt_{1iii}/graphene. Thus, we concluded that $^*COOH$ did not immediately react with $^*H$ to form $^*HCOOH$ on three 2H-Pt_1/graphene configurations, but rather dissociated H_2 first, followed by $^*COOH$ reacting with dissociated $^*H$ to form $^*HCOOH$. The $^*HCOOH$ was likely to react further with $^*H$ or to desorb from the Pt site. The hydrogenation of $^*HCOOH$ to $^*H_2COOH$ showed a higher energy than $^*HCOOH$ desorption on three 2H-Pt_1/graphene configurations, suggesting that $^*HCOOH$ would desorb rather than further hydrogenate.

Although three 2H-Pt_1/graphene configurations followed the same pathway to hydrogenate CO_2 into HCOOH, the rate-determining step (RDS) varied structures. For 2H-Pt_{1i}/graphene and 2H-Pt_{1iii}/graphene, the RDS was $^*H_2 \rightarrow 2^*H$, with energy barriers of 1.22 and 1.02 eV, respectively. In contrast, for 2H-Pt_{1ii}/graphene, the RDS was $^*COOH+^*H \rightarrow ^*HCOOH$, with an energy barrier of 0.66 eV Among the three 2H-Pt_1/graphene configurations, 2H-Pt_{1ii}/graphene showed the lowest RDS energy barriers for CO_2 hydrogenation to HCOOH.

For the three 2H-2OH-Pt_2/graphene configurations, Pt_2 dimers acted as the active sites for CO_2 hydrogenation. The CO_2 molecules were physically adsorbed on 2H-2OH-Pt_2/graphene, with adsorption free energies of 0.30, 0.41, and 0.43 eV for 2H-2OH-Pt_{2i}/graphene, 2H-2OH-Pt_{2ii}/graphene, and 2H-2OH-Pt_{2iii}/graphene, respectively. After adsorption on the surface, CO_2 will undergo gradual hydrogenation to form CH_3OH. The reaction pathways for CO_2 hydrogenation to CH_3OH over 2H-2OH-Pt_{2i}/graphene, 2H-2OH-Pt_{2ii}/graphene, and 2H-2OH-Pt_{2iii}/graphene were illustrated in Fig. 3, Figs. S16 and S17 (Supporting information), respectively. Considering that the optimal hydrogenation pathway for CO_2 over three 2H-2OH-Pt_2/graphene configurations was similar, we used 2H-2OH-Pt_{2i}/graphene as an illustrative example to analyze the detailed reaction pathway.

In the reaction process, the adsorption of CO_2 was followed by hydrogenation to form $^*COOH$ or $^*HCOO$ intermediates (Fig. 3). The energy barrier to generate $^*COOH$ on 2H-2OH-Pt_{2i}/graphene was 0.71 eV, which was lower than that for $^*HCOO$ (1.37 eV), indicating that CO_2 preferentially generated $^*COOH$. Following the generation of $^*COOH$, an H_2 molecule adsorbed on the Pt_{top} atoms, which then dissociated into two $^*H$ species. One of the $^*H$ atoms on the Pt_{top} atoms migrated to the non-top Pt atoms (named as $Pt_{non\text{-}top}$) with an energy barrier of 0.04 eV. In this stage, the $Pt_{non\text{-}top}$ atoms adsorbed one H species, while the Pt_{top} atoms adsorbed two H species and one $^*COOH$ species. One of the $^*H$ atoms on the Pt_{top} atoms combined with $^*COOH$ to form $^*C(OH)_2$ or $^*HCOOH$ species. The formation of $^*C(OH)_2$ exhibited a lower energy barrier (0.86 eV) than $^*HCOOH$ formation (1.12 eV), suggesting that H preferred to combine with $^*COOH$ to form $^*C(OH)_2$ species.

When the $^*C(OH)_2$ species were formed, the $^*H$ atom on the $Pt_{non\text{-}top}$ atoms migrated to the Pt_{top} atoms with a migration barrier of 0.69 eV Subsequently, the $^*H$ atom on the Pt_{top} site reacted with $^*C(OH)_2$, generating $^*CH(OH)_2$ with an energy barrier of 0.33 eV. A second H_2 molecule adsorbed onto the Pt_{top} sites and dissociated into two $^*H$ atoms. Afterward, one $^*H$ atom migrated from the Pt_{top} sites to the $Pt_{non\text{-}top}$ sites, and the $^*CH(OH)_2$ species combined with the $^*H$ on the Pt_{top} atoms, breaking the C–O bond and forming an $^*H_2O$ molecule with an energy barrier of 0.82 eV. However, the $^*H_2O$ molecule was unstable and desorbed from the Pt_{top} sites. After desorption of H_2O, one $^*HCOH$ species and one $^*H$ species remained on the Pt_{top} atom. The $^*H$ on the $Pt_{non\text{-}top}$ atom transferred to the Pt_{top} sites with an energy barrier of 0.22 eV. One of the $^*H$ atoms on the Pt_{top} atom combined with $^*HCOH$ to form $^*CH_2OH$ species. A third H_2 molecule physically adsorbed onto the Pt_{top} sites and dissociated into two H atoms with a low energy barrier of 0.60 eV, and one of the $^*H$ atoms on the Pt_{top} sites reacted with $^*CH_2OH$ to generate $^*CH_3OH$ products. The RDS of three 2H-2OH-Pt_2/graphene configurations were the dissociation of the first H_2 molecules, with energy barriers of 0.93, 0.87, and 0.87 eV for 2H-2OH-Pt_{2i}/graphene, 2H-2OH-Pt_{2ii}/graphene, and 2H-2OH-Pt_{2iii}/graphene, respectively. Three Pt_2/graphene configurations exhibited similar RDS energy barriers.

Based on the above discussion, it was observed that three Pt_1/graphene configurations tended to produce HCOOH, whereas three Pt_2/graphene configurations preferred CH_3OH. To investigate the differences in product selectivity between Pt_2/graphene and Pt_1/graphene, we chose Pt_{1ii}/graphene and Pt_{2i}/graphene as examples to analyze the hydrogenation pathways of the $^*COOH$ intermediates. As shown in Fig. 4a, the Pt atoms of Pt_{1ii}/graphene adsorbed three $^*H$ and one $^*COOH$ species. The combination of $^*H$ and $^*COOH$ on Pt_{1ii}/graphene resulted in the formation of $^*HCOOH$ with an energy barrier of 0.66 eV, which was lower than that for $^*C(OH)_2$ formation (0.75 eV). The result indicated that $^*COOH$ would directly react with $^*H$ to produce $^*HCOOH$ on Pt_{1ii}/graphene.

For Pt_{2i}/graphene (Fig. 4b), the Pt_{top} atoms also adsorbed three $^*H$ and one $^*COOH$ species. Nevertheless, $^*H$ did not directly react with $^*COOH$. Instead, it migrated to the $Pt_{non\text{-}top}$ atoms with an energy barrier of 0.04 eV. Subsequently, one of the $^*H$ atoms on the Pt_{top} atoms combined with $^*COOH$ to form $^*HCOOH$ or $^*C(OH)_2$. The formation of $^*C(OH)_2$ exhibited a lower energy barrier (0.86 eV) compared to the generation of $^*HCOOH$ (1.12 eV), suggesting that $^*COOH$ species on Pt_{2i}/graphene were more likely to undergo hydrogenation to generate $^*C(OH)_2$ species. Thus, the difference in selectivity between Pt_1/graphene and Pt_2/graphene derived from the migration of $^*H$ from the Pt_{top} atoms to the $Pt_{non\text{-}top}$ atoms, altering the pathway of CO_2 hydrogenation.

The catalytic reactivity of Pt_1/graphene and Pt_2/graphene catalysts for CO_2 hydrogenation processes was further assessed using microkinetic simulations. The reaction conditions were set to be the same as those in previous works [32,33], with specifics detailed in Tables S1 and S2 (Supporting information), as well as computational methods. The microkinetic simulation results for Pt_1/graphene and Pt_2/graphene catalysts were presented in Fig. 5.

For the three Pt_1/graphene catalysts, there is a significant difference in TOF values for the generation of HCOOH (Fig. 5a). Among them, Pt_{1ii}/graphene exhibited the highest TOF value of 744.48 h^{-1}, which was comparable to that previously reported value (780.7 h^{-1}) [33] under identical reaction conditions ($T = 473.15$ K, $P = 4.50$ MPa, and H_2/CO_2 ratio of 3:1). To explore the reason for the superior activity of Pt_{1ii}/graphene compared to Pt_{1i}/graphene and Pt_{1iii}/graphene, we investigated the center of d-

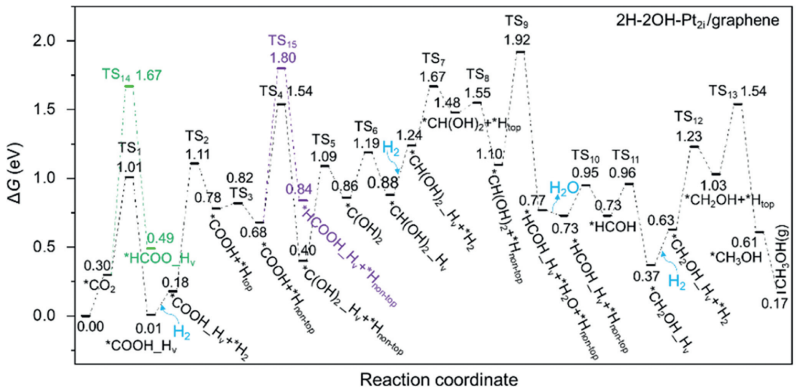

Fig. 3. The free energy profiles for the hydrogenation of CO_2 to CH_3OH on 2H-2OH-Pt_{2i}/graphene, and the corresponding intermediate structures were shown in Fig. S15 (Supporting information). TS represented the transition state. The black route was the most possible reaction pathway for CO_2 hydrogenation to CH_3OH on 2H-2OH-Pt_{2i}/graphene. H_v represented one H atom was missing from 2H-2OH-Pt_{2i}/graphene structure after it binds to intermediate. $^*H_{top}$ and $^*H_{non\text{-}top}$ represented H atoms adsorbed on Pt_{top} sites and $Pt_{non\text{-}top}$ sites, respectively.

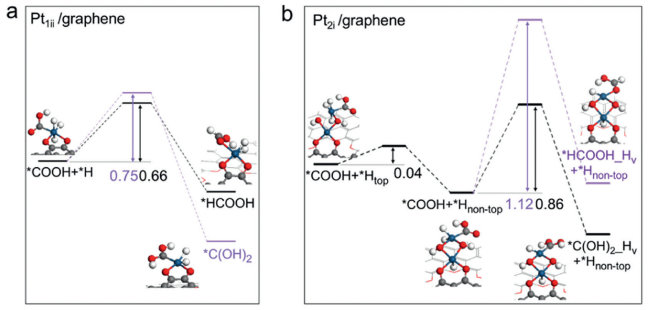

Fig. 4. The free energy barriers for $^*COOH$ hydrogenation to $^*HCOOH$ and $^*C(OH)_2$ over (a) Pt_{1ii}/graphene and (b) Pt_{2i}/graphene.

orbitals (ε_d) of the metal. The ε_d for Pt atoms in 2H-Pt_{1i}/graphene, 2H-Pt_{1ii}/graphene and 2H-Pt_{1iii}/graphene were −1.21, −1.11, and −1.98 eV, respectively (Fig. 6a). Notably, the ε_d of 2H-Pt_{1ii}/graphene was closer to the Fermi level than that of 2H-Pt_{1i}/graphene and 2H-Pt_{1iii}/graphene, which facilitated faster electron transfer and thereby enhancing the catalytic activity for CO_2 hydrogenation to HCOOH.

For three Pt_2/graphene catalysts, the TOF values for the formation of CH_3OH varied significantly (Fig. 5b). Among these catalysts, Pt_{2i}/graphene showed the highest TOF value (789.48 h^{-1}), which was magnitude larger than of a previously reported Ir-based catalyst (0.15 h^{-1}) [32] under the same reaction conditions (T = 353.15 K, P = 4.0 MPa, and H_2/CO_2 ratio of 3:1). To investigate the underlying cause of the enhanced activity of Pt_{2i}/graphene compared to Pt_{2ii}/graphene and Pt_{2iii}/graphene, we calculated the

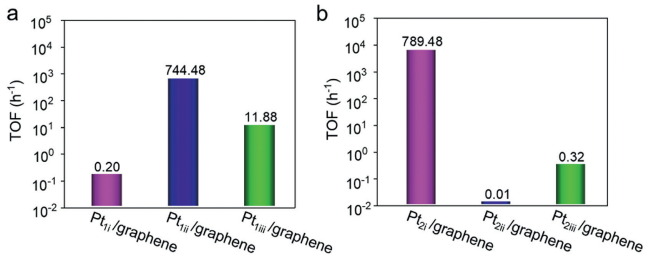

Fig. 5. The results of microkinetic simulations. (a) Turnover frequency (TOF) for HCOOH formation on Pt_1/graphene from the catalytic CO_2 hydrogenation reaction. T = 473.15 K, P = 4.5 MPa and H_2/CO_2 ratio of 3:1. (b) TOF for CH_3OH formation on Pt_2/graphene from the catalytic CO_2 hydrogenation reaction. T = 353.15 K, P = 4.0 MPa and H_2/CO_2 ratio of 3:1.

distance and the integrated crystal orbital Hamilton population (ICOHP) between Pt_{top} and $Pt_{non\text{-}top}$ to evaluate their interaction. As shown in Figs. 6b-d, 2H-2OH-Pt_{2i}/graphene exhibited a shorter distance between Pt_{top} and $Pt_{non\text{-}top}$ (2.773 Å) than 2H-2OH-Pt_{2ii}/graphene (3.105 Å) and 2H-2OH-Pt_{2iii}/graphene (3.109 Å). Furthermore, the calculated ICOHP value between Pt_{top} and $Pt_{non\text{-}top}$ for 2H-2OH-Pt_{2i}/graphene was −0.13 eV, which was more negative than that for 2H-2OH-Pt_{2ii}/graphene (−0.03 eV) and 2H-2OH-Pt_{2iii}/graphene (−0.06 eV). These results indicated that the closer Pt-Pt distance in 2H-2OH-Pt_{2i}/graphene enhanced the interaction between two adjacent Pt atoms, thus accelerating the electron transfer in the process of kinetic transformation and improving the catalytic activity [34].

To assess the stability of 2H-Pt_{1ii}/graphene and 2H-2OH-Pt_{2i}/graphene, we performed *ab initio* molecular dynamics simu-

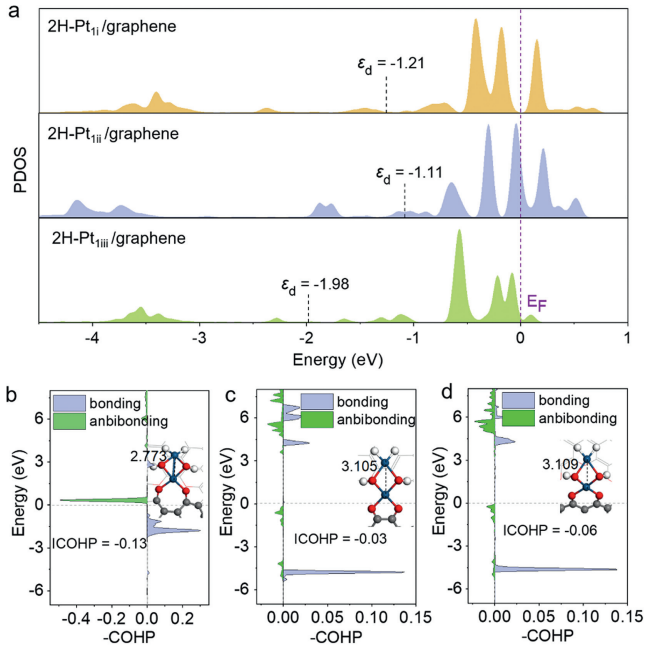

Fig. 6. (a) PDOS of Pt d-orbitals and the corresponding d-orbitals center for three 2H-Pt_1/graphene structures. The Fermi level (E_F) was set to 0 eV. The integrated crystal orbital Hamilton population (ICOHP) between Pt_{top} and $Pt_{non\text{-}top}$ of (b) 2H-2OH-Pt_{2i}/graphene, (c) 2H-2OH-Pt_{2ii}/graphene and (d) 2H-2OH-Pt_{2iii}/graphene. The distance depicted in the illustration represented the separation between Pt_{top} and $Pt_{non\text{-}top}$, measured in Å.

lations at 473 K for 2H-Pt_{1ii}/graphene and at 353 K for 2H-2OH-Pt_{2i}/graphene. The simulations lasted for 6 ps with a time-step of 1 fs. The geometric structures of both 2H-Pt_{1ii}/graphene and 2H-2OH-Pt_{2i}/graphene showed no significant distortion during the simulations, indicating their high thermodynamic stability under reaction conditions (Fig. S18 in Supporting information).

In conclusion, we investigated the catalytic performance of Pt_1/graphene and Pt_2/graphene for CO_2 hydrogenation, and observed that Pt_1/graphene configurations favored the conversion of CO_2 into HCOOH, whereas CO_2 was hydrogenated into CH_3OH on Pt_2/graphene. The distinct product selectivity between Pt_1/graphene and Pt_2/graphene originated from the synergistic interaction of Pt_2 dimers, which hydrogenated *COOH into $*C(OH)_2$ instead of *HCOOH, altering the hydrogenation pathway of CO_2. Additionally, Pt_{1ii}/graphene and Pt_{2i}/graphene showed high activity for CO_2 hydrogenation with TOF values of 744.48 h^{-1} and 789.48 h^{-1}, respectively. This work paves the way for manipulating catalytic properties and advancing the mechanistic understanding of heterogeneous catalysis.

Declaration of competing interest

The authors declare that they have no known competing financial interests or personal relationships that could have appeared to influence the work reported in this paper.

CRediT authorship contribution statement

Sanmei Wang: Writing – review & editing, Writing – original draft, Software, Methodology, Investigation, Formal analysis, Data curation. **Dengxin Yan:** Software, Methodology, Data curation. **Wenhua Zhang:** Writing – review & editing, Supervision, Software, Funding acquisition, Data curation. **Liangbing Wang:** Writing – review & editing, Supervision, Funding acquisition.

Acknowledgments

This work was supported by the National Key Research and Development Program (No. 2022YFA1505800), the National Natural Science Foundation of China (No. 22373092), CAS Project for Young Scientists in Basic Research (No. YSBR-051). China Association for Science and Technology (No. YESS20200031), the Start-up Funding of Central South University (No. 502045005), and Industry-University-Research Cooperation Projects with Zhejiang NHU Co., Ltd., and Ningbo Fengcheng Advanced Energy Materials Research Institute. Wenhua Zhang is supported by USTC Tang Scholarship. The calculations were performed on the Super-computing Center of University of Science and Technology of China (USTC-SCC).

Supplementary materials

Supplementary material associated with this article can be found, in the online version, at doi:10.1016/j.cclet.2024.110611.

References

[1] J. Rogelj, M. den Elzen, N. Höhne, et al., Nature 534 (2016) 631–639.
[2] J.D. Shakun, P.U. Clark, F. He, et al., Nature 484 (2012) 49–54.
[3] S. Jin, Z. Hao, K. Zhang, et al., Angew. Chem. Int. Ed. 60 (2021) 20627–20648.
[4] L. Li, F. Chen, B. Zhao, Y. Yu, Chin. Chem. Lett. 35 (2024) 109240.
[5] Q. Cheng, M. Huang, Q. Ye, et al., Chin. Chem. Lett. 35 (2024) 109112.
[6] H. Zhang, Q. Liu, Z. Shen, Chin. Chem. Lett. 35 (2024) 108607.
[7] T. Jia, L. Wang, Z. Zhu, et al., Chin. Chem. Lett. 35 (2024) 108692.
[8] G.A. Olah, G.K.S. Prakash, A. Goeppert, J. Am. Chem. Soc. 133 (2011) 12881–12898.
[9] X. Duan, J. Xu, Z. Wei, et al., Adv. Mater. 29 (2017) 1701784.
[10] R.P. Ye, J. Ding, W. Gong, et al., Nat. Commun. 10 (2019) 5698.
[11] F. Wang, S. Zhang, W. Jing, et al., J. Mater. Sci. Technol. 189 (2024) 146–154.
[12] G. Glockler, J. Phys. Chem. 62 (1958) 1049–1054.
[13] S. Wang, Q. Li, Y. Xin, et al., Nanoscale 15 (2023) 6999–7005.
[14] T. Yang, X. Mao, Y. Zhang, et al., Nat. Commun. 12 (2021) 6022.
[15] K.W. Ting, T. Toyao, S.M.A.H. Siddiki, K.I. Shimizu, ACS Catal. 9 (2019) 3685–3693.
[16] Y. Chen, H. Li, W. Zhao, et al., Nat. Commun. 10 (2019) 1885.
[17] Y. Hu, H. Li, Z. Li, et al., Green Chem. 23 (2021) 8754–8794.
[18] T. Liu, W. Zhang, Q. Tan, et al., Chem. Eng. J. 489 (2024) 150286.
[19] H. Shi, H. Wang, Y. Zhou, et al., Angew. Chem. Int. Ed. 61 (2022) e202208904.
[20] H. Li, L. Wang, Y. Dai, et al., Nat. Nanotechnol. 13 (2018) 411–417.
[21] Z. Zeng, L.Y. Gan, H.Bin Yang, et al., Nat. Commun. 12 (2021) 4088.
[22] Y. Lou, F. jiang, W. Zhu, et al., Appl. Catal. B: Environ. 291 (2021) 120122.
[23] W. Zhang, T. Liu, Q. Tan, et al., ACS Catal. 13 (2023) 3242–3253.
[24] X. Wan, Y. Li, Y. Chen, et al., Nat. Commun. 15 (2024) 1273.
[25] W. Ren, X. Tan, W. Yang, et al., Angew. Chem. Int. Ed. 58 (2019) 6972–6976.
[26] Y. Wang, B.J. Park, V.K. Paidi, et al., ACS Energy Lett. 7 (2022) 640–649.
[27] G. Sun, Y. Cao, D. Li, et al., Appl. Catal. A: Gen. 651 (2023) 119025.
[28] Y. Si, Y. Jiao, M. Wang, et al., Nat. Commun. 15 (2024) 4887.
[29] X. Chen, M. Peng, X. Cai, et al., Nat. Commun. 12 (2021) 2664.
[30] Y. Sun, S. Wang, D. Jiao, et al., Chin. Chem. Lett. 33 (2022) 3987–3992.
[31] H. Yan, Y. Lin, H. Wu, et al., Nat. Commun. 8 (2017) 1070.
[32] R. Kanega, N. Onishi, S. Tanaka, et al., J. Am. Chem. Soc. 143 (2021) 1570–1576.
[33] Z. Wang, Y. Kang, J. Hu, et al., Angew. Chem. Int. Ed. 62 (2023) e202307086.
[34] Y. Hu, Z. Li, B. Li, C. Yu, Small 18 (2022) 2203589.